J Mater Sci (2019) 54:10284–10296

Computation and theory

Stability and physical properties tuning via interstitials chemical engineering of Zr_5Sn_3: a first-principles study

Hongmei Chen[1], Yu Cao[1], Ke Liu[1], Xiaoma Tao[1], Yulu Zhou[1], Yifang Ouyang[1,*], Fei Gao[2], Yong Du[3], and Qing Peng[2,*]

[1] Guangxi Colleges and Universities Key Laboratory of Novel Energy Materials and Related Technology, College of Physical Science and Technology, Guangxi University, Nanning 530004, China
[2] Department of Nuclear Engineering and Radiological Science, University of Michigan, Ann Arbor, MI 48109, USA
[3] State Key Laboratory of Powder Metallurgy, Central South University, Changsha 410083, China

Received: 27 November 2018
Accepted: 11 April 2019
Published online: 16 April 2019

ABSTRACT

Hexagonal binary intermetallics A_5B_3 has a unique A_6 octahedra chain structure, providing space for interstitial chemical engineering the physical, mechanical, electrical, and chemical properties without change in the basic structure of crystal. Because of the engineering importance of Zr–Sn alloy, here, we investigate the influence of 24 interstitial alloying elements X (X = B, C, N, O, Al, Si, P, S, Sc, Ti, V, Cr, Mn, Fe, Co, Ni, Cu, Zn, Ga, Ge, As, Se, Nb, and Sn) on stability and properties of hexagonal Zr_5Sn_3 via first-principles calculations. A general trend is that the additional element with small atom size and high electronegativity is favorable as interstitials in Zr_5Sn_3. The calculated formation enthalpy and the elastic constants suggest that these Zr_5Sn_3X structures are thermodynamically and mechanically stable. The calculated phonon spectra indicate that Zr_5Sn_3X structures are dynamically stable except X = V, Cr, Mn, Zn, and Nb. We show that their electronic structures including bonding characters have strong correlation with the stability and mechanical properties. With strong covalent bonds, Zr_5Sn_3B has the highest Young's modulus, bulk modulus, shear modulus, Debye temperature, and microhardness. The addition of alloying elements decreases the anisotropy except X = O, Sc, Ti, V and Nb. All the additive elements increase the specific heat capacity of Zr_5Sn_3. Our results could be helpful in designing and improve the performance of Zr–Sn alloy on demand.

Address correspondence to E-mail: ouyangyf@gxu.edu.cn; qpeng.org@gmail.com

https://doi.org/10.1007/s10853-019-03622-5

Introduction

Zirconium alloys containing 1.2–1.7 at.% Sn and small addition of other elements (such as Fe, Ni, Cu, Cr, and Nb) are important structural materials with an extensive applications due to the excellent radiation resistance, corrosion resistance, and mechanical properties [1, 2]. The phase-diagram and associated properties of Zr–Sn binary system have been extensively studied by experiments [3–8] and theory [9]. One of the Zr–Sn intermetallic compounds Zr_5Sn_3 attracted more attention due to its special polar structure (see [10]). As a polar intermetallic compound, Zr_5Sn_3 belongs to the Mn_5Si_3 structural family ($P6_3/mcm$, space group #193, hexagonal crystal, as shown in Fig. 1) in which confacial octahedra of the transition element form quasi-infinite chains. The added interstitial element X (X represents elements with frame in element period table as shown in Fig. 1) in the octahedra of Zr_5Sn_3 results in the formation of Zr_5Sn_3X (similarly as Zr_5Sb_3X, which provides some potential applications [11]). Some Zr_5Sn_3X (X = B, C, O, Al, Si, P, S, Cu, Zn, Ga, Ge, As, Fe, Co, and Ni) compounds have been synthesized and found that their structural properties depend strongly on the preparation method and the compositions [12–14]. Besides the applications in nuclear energy, it is also suggested Zr_5Sn_3X (X = Li and Mg) for anode material for magnesium- and lithium-ion batteries [15].

The dependence of properties of Zr_5Sn_3 on alloying elements is an open question and critical in designing Zr–Sn alloy. In this paper, we study the structural stability and elastic properties of Zr_5Sn_3X (X = B, IVA, N, O, Al, 3d_TM, Nb and Sn) using first-principles calculations. The dependence of thermodynamic and physical properties on alloying elements has been investigated. Our results could be helpful in fundamental understanding the effects of alloying elements on the properties of Zr_5Sn_3 and extend their applications.

Methods

First-principles calculations of the total energy, electronic structure, and elastic constant are performed by PAW pseudopotential formalism [16, 17] as implemented in VASP soft package [18, 19] with GGA [20]. An energy cutoff of 450 eV is used for the all study of the Zr_5Sn_3X compound. Brillöuin zone integrations employ Monkhorst–Pack *k*-point meshes [21], and the Methfessel–Paxton technique [22] with a smearing parameter of 0.1 eV. The reciprocal space (*k*-point) meshes are chosen to achieve convergence to a precision of 1.0 meV/atom. The total energy convergence is better than 1×10^{-6} eV/unit with full relaxation. The forces are converged to less than 0.01 eV/Å. The phonon dispersion curves were calculated using the supercell approach. Force constants of supercell have been obtained using the VASP code, and the PHONOPY code [23, 24] has been performed to calculate the phonon frequencies and phonon density of states. For the phonon dispersion calculation, we use the $2 \times 2 \times 2$ supercell containing 144

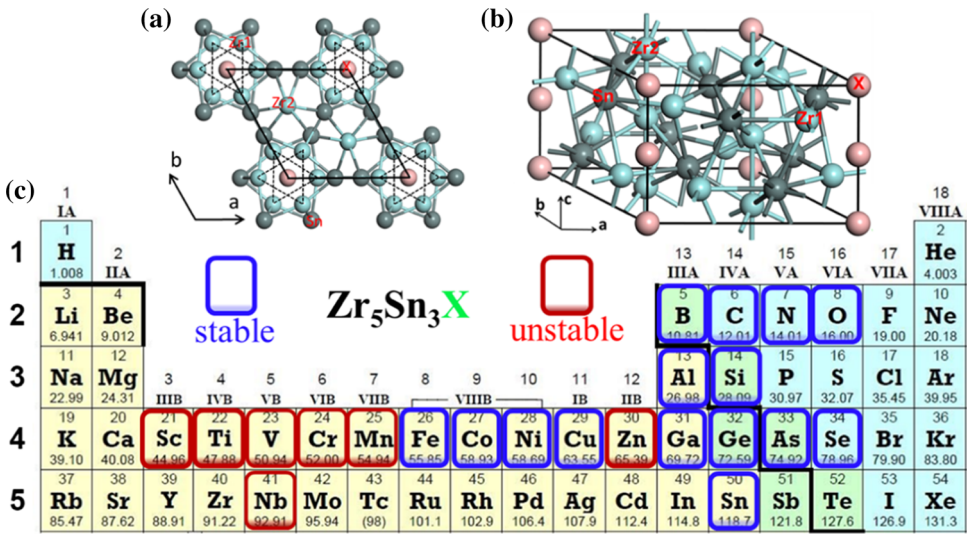

Figure 1 Host structure and the additional element X. **a** Crystal structure of Zr_5Sn_3 in [001] projection and **b** side view. Two types of Zr atoms are labeled differently for distinction. The octahedral site is shown by the dashed line. **c** Overview the stabilities of the 24 additional interstitial element Xs in the frame of periodic table denoted by blue box (stable) and red box (unstable).

atoms for Zr_5Sn_3X and the 3 × 3 × 5 Monkhorst–Pack k-point mesh for the BZ integration.

The Birch–Murnaghan [25] equation of state is used to obtain the equilibrium volume (Ω_0), the total energy (E), the bulk modulus (B), and the pressure derivative of the bulk modulus ($\partial B/\partial P$). The formation enthalpies (ΔH) of the Zr_5Sn_3X compound can be, respectively, calculated by the following equations:

$$\Delta H(Zr_5Sn_3X) = \frac{1}{9}[E(Zr_5Sn_3X) - E(X) - 3E(Sn) - 5E(Zr)] \quad (1)$$

where $E(Zr_5Sn_3X)$, $E(Zr_5Sn_3)$, $E(X)$, $E(Sn)$, and $E(Zr)$ are the equilibrium total energies of the Zr_5Sn_3X, Zr_5Sn_3, element X, Sn, and Zr, respectively. The excess Gibbs free energy between Zr_5Sn_3X and the mixture of Zr_5Sn_3 and X can be evaluated as

$$\Delta G_{Zr_5Sn_3X}(T,P) = \frac{1}{9}[G_{Zr_5Sn_3X}(T,P) - G_X(T,P) - G_{Zr_5Sn_3}(T,P)] \quad (2)$$

The Gibbs free energy for Zr_5Sn_3X, Zr_5Sn_3, and X was obtained by quasi-harmonic Debye model [26].

The elastic constants can be obtained by calculating the total energy as a function of strains. For a hexagonal material, there are five independent single-crystal elastic constants, namely C_{11}, C_{12}, C_{13}, C_{33}, and C_{44}. The details of the calculations can be found in Refs. [27, 28]. The effective elastic moduli of polycrystalline aggregates are usually calculated by two approximations due to Voigt [29] and Reuss [30] in which, respectively, uniform strain or stress are assumed throughout the polycrystal. Hill [31] showed that the Voigt and Reuss averages are limits and suggested that the actual effective moduli could be obtained by the arithmetic mean of the two bounds. The Young's modulus and the Poisson's ratio can be evaluated from the bulk and shear moduli [28].

Results

Charge transfer

In order to obtain more information on the electron charge distribution and charge transfer between the atoms and to elucidate the type of the chemical bonds, the Bader's electronic analysis in molecule theory was used [32], and the results are plotted in Fig. 2. It should be noted the Bader's charges were calculated using charges of atoms in IMCs minus charges of atom in its bulk of the ground state. Bader's theory predicts a charge transfer from Zr to X (except X = Sc and Ti) and Sn atom, with the largest amount of charge transfer in Zr_5Sn_3C and the least amount of charge transfer in Zr_5Sn_3Nb, which is coincident with the stability of Zr_5Sn_3X. The transfer of Bader's charge from the element X (except X = Cr and Mn) is positively correlated with the stability of the Zr_5Sn_3X.

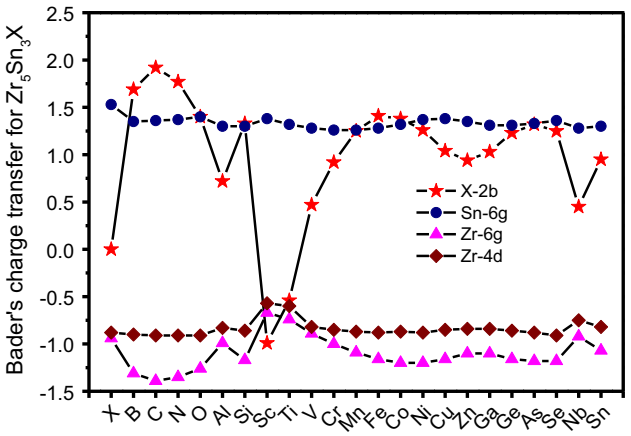

Figure 2 Charge transfer of Zr_5Sn_3X.

Formation enthalpy

The calculated lattice constants and formation enthalpies are reported in Table 1 including available experimental data [14, 33, 34]. For the Zr_5Sn_3, Zr_5Sn_4, Zr_5Sn_3B, Zr_5Sn_3C, Zr_5Sn_3N, Zr_5Sn_3O, Zr_5Sn_3Si, Zr_5Sn_3Ge, Zr_5Sn_3Zn, Zr_5Sn_3Ga, Zr_5Sn_3Se, Zr_5Sn_3Al, Zr_5Sn_3Cu, and Zr_5Sn_3Fe systems, the present optimized structural parameters (at 0 K) are in good agreement with the available experimental lattice constants [14, 33, 34]. However, the present calculated lattice constants are slightly larger than the experimental data, which is a common error inherent to GGA calculations. The calculated formation enthalpies of the considered compounds are all negative, which indicates that these compounds are energetically stable relative to pure constituents. The calculated formation enthalpies for Zr_5Sn_3 and Zr_5Sn_4 are in agreement with available experimental [35] and theoretical data [6–9]. The thermodynamical stability is ultimately governed by the excess Gibbs free energy. For that, we considered the excess Gibbs formation

Table 1 Lattice constants (in Å), formation enthalpies (in eV/atom), Poisson's ratio, B/G ratio, hardness (in GPa), Debye temperature (in Kelvin), and elastic anisotropy of Zr_5Sn_3X

Alloy	*a*	*c*	*c/a*	ΔH	*v*	*B/G*	H_v	Θ	A_B	A_G	A_U	References
Zr_5Sn_3	8.5445	5.8106	0.6800	− 0.5575	0.281	1.94	6.48	316.7	0.357	2.639	0.278	Present
	8.462	5.797										[33]
				− 0.738								[35]
				− 0.577								[6]
				− 0.572	0.288	2.03						[9]
				− 0.771								[7]
Zr_5Sn_3B	8.5762	5.8366	0.6806	− 0.6695	0.211	1.40	14.41	393.6	0.180	0.165	0.020	Present
	8.4936	5.8029	0.683									[14]
Zr_5Sn_3C	8.5115	5.8548		− 0.6979	0.235	1.56	11.62	377.0	0.016	0.229	0.023	Present
	8.4268	5.8001	0.688									[14]
Zr_5Sn_3N	8.4794	5.7978		− 0.8584	0.277	1.91	8.37	373.3	0.074	0.589	0.061	Present
Zr_5Sn_3O	8.4756	5.7748		− 1.0419	0.257	1.72	9.27	358.2	0.108	3.472	0.362	Present
	8.4256	5.763	0.684									[14]
Zr_5Sn_3Al	8.7365	5.9084	0.6763	− 0.5961	0.234	1.55	11.28	367.5	0.111	0.305	0.033	Present
	8.655	5.871	0.678									[14]
Zr_5Sn_3Si	8.7006	5.8897		− 0.7122	0.225	1.49	12.64	380.7	0.159	0.044	0.008	Present
	8.6072	5.844	0.679									[14]
Zr_5Sn_3Sc	8.7757	6.0313		− 0.4549	0.303	2.20	4.43	300.5	0.136	3.913	0.410	Present
Zr_5Sn_3Ti	8.7320	5.9318		− 0.4118	0.296	2.12	5.24	313.5	0.007	5.179	0.546	Present
Zr_5Sn_3V	8.7196	5.8833		− 0.3990	0.320	2.44	3.44	292.9	0.045	6.748	0.725	Present
Zr_5Sn_3Cr	8.7149	5.8516		− 0.4016	0.326	2.54	3.24	295.8	0.294	1.891	0.199	Present
Zr_5Sn_3Mn	8.7138	5.8460		− 0.4654	0.306	2.25	4.87	317.6	0.040	1.259	0.128	Present
Zr_5Sn_3Fe	8.7096	5.8350	0.6699	− 0.5022	0.262	1.77	8.51	344.4	0.293	0.505	0.057	Present
	8.671	5.884	0.678									[14]
Zr_5Sn_3Co	8.6955	5.8287		− 0.5596	0.270	1.84	7.77	336.8	0.763	0.310	0.033	Present
Zr_5Sn_3Ni	8.6691	5.8782	0.6781	− 0.5657	0.275	1.89	7.24	332.2	0.380	0.253	0.033	Present
Zr_5Sn_3Cu	8.6777	5.8888	0.6786	− 0.5374	0.262	1.77	8.53	343.3	0.293	0.505	0.057	Present
	8.6249	5.877	0.681									[14]
Zr_5Sn_3Zn	8.7066	5.9044		− 0.5774	0.236	1.56	11.20	361.7	0.181	0.379	0.042	Present
	8.6325	5.877	0.681									[14]
Zr_5Sn_3Ga	8.7217	5.9084		− 0.6520	0.195	1.31	15.01	367.9	0.610	0.931	0.106	Present
	8.6599	5.8794	0.679									[14]
Zr_5Sn_3Ge	8.7255	5.9146		− 0.7046	0.214	1.42	13.10	362.5	0.177	0.048	0.008	Present
	8.6414	5.866										[14]
Zr_5Sn_3As	8.6922	5.9693		− 0.7722	0.270	1.84	8.44	353.7	0.089	1.169	0.120	Present
	8.6037	5.9200	0.688									[14]
Zr_5Sn_3Se	8.6459	6.0667		− 0.7918	0.243	1.62	10.49	355.5	0.501	0.286	0.039	Present
	8.5584	5.9515	0.695									[14]
Zr_5Sn_3Nb	8.7723	5.9214	0.6750	− 0.4246	0.296	2.12	5.34	309.3	0.007	3.449	0.357	Present
Zr_5Sn_4	8.8477	5.9794	0.6758	− 0.5834	0.251	1.67	9.38	336.1	0.021	0.344	0.035	Present
	8.759	5.916										[34]
				− 0.606								[6]
				− 0.601	0.265	1.80						[9]
				− 0.820								[7]

free energy, which is the free energy difference between the Zr_5Sn_3X and the mixture of Zr_5Sn_3 and *X*. We calculate the excess Gibbs free energy using the quasi-harmonic Debye method and the excess Gibbs formation free energy (ΔG_{ex}) of Zr_5Sn_3X relative to the mixture of Zr_5Sn_3 and X is demonstrated in

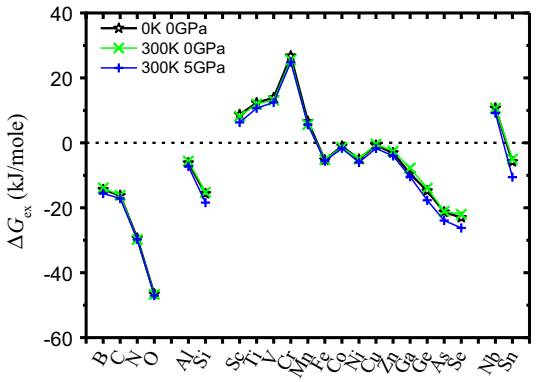

Figure 3 Excess formation free energy of Zr_5Sn_3X varies as added element under different temperature and pressure. The effect of temperature and pressure on the excess formation free energy is slight. The excess formation free energy of Zr_5Sn_3O is the lowest and it indicates the most stable relative to Zr_5Sn_3 and O_2. The excess formation free energies of Zr_5Sn_3X (X = Sc, Ti, V, Cr, Mn and Nb) are positive and unstable relative to Zr_5Sn_3 and X.

Fig. 3 (and Figure S1 in Supplementary Information) under different conditions (0 K 0 GPa, 300 K 0 GPa and 5 GPa). The minus ΔG_{ex} indicates stability of Zr_5Sn_3X compared with Zr_5Sn_3. One can see that the Zr_5Sn_3X are stable except X = Sc, Ti, V, Mn, Cr, and Nb. The effects of temperature and pressure are different for different elements. There is a similar trend of the variation of the excess Gibbs formation free energy in response to temperature and pressure for all X in the Zr_5Sn_3X structures. As for X = Sc, Ti, V, Mn, Cr, and Nb, whose excess Gibbs free energy is positive at 0 K and 0 GPa, it turns to negativity when the pressure is more than some value (40 GPa for X = Nb), which indicates that Zr_5Sn_3Nb is more stable than the mixture of Zr_5Sn_3 and Nb under high pressure over 40 GPa.

Dynamic stability

The stability of IMCs is also dynamically determined by the phonon dispersion curves. The vibrational phonon spectra for Zr_5Sn_3X have been calculated, and some spectra of Zr_5Sn_3 and Zr_5Sn_3X (X = B, Nb and Sn) are demonstrated in Fig. 4, and the rest (X = C, O, Al, Si, P, S, Cu, Zn, Ga, Ge, As, Sc, Ti, V, Cr, Mn, Fe, Co and Ni) are displayed in Figure S2 in Supplementary Information. One can see that the phonon dispersion curves indicate the dynamical stability except Zr_5Sn_3Nb, for which, there is imagine frequencies along the symmetric directions Γ–K and Γ–M. This indicates that Zr_5Sn_3Nb is dynamically unstable. From the calculated phonon spectra, the systems of Zr_5Sn_3X (X = V, Cr, Mn, Nb and Zn) are dynamically unstable.

Elastic properties

Elastic properties (bulk modulus, shear modulus, Young's modulus, and Poisson's ratio) of a solid are essential part of the mechanical properties. The elastic constants of the Zr_5Sn_3X phases have been calculated as summarized in Fig. 5. The calculated elastic constants of Zr_5Sn_3 and Zr_5Sn_4 agree well with other theoretical results [6, 9]. For the hexagonal system, the mechanical stability criteria are given by $C_{44} > 0$, $C_{11} > |C_{12}|$, and $(C_{11} + 2C_{12})C_{33} > 2C_{13}$ [2]. The calculated elastic constants of the Zr_5Sn_3X satisfy these stability conditions. From Fig. 5, one can see $C_{11} < C_{33}$ for Zr_5Sn_3 and Zr_5Sn_3X (X = C, N, O, Sc, Ti, V, Mn and Nb), which indicates that the bonding strength along the [100] and [010] direction is weaker than that of the bonding along the [001] direction. The bulk modulus, Young's modulus and shear modulus have been estimated from the calculated single-crystal elastic constants as presented in Fig. 5. The Young's modulus (E) is intrinsic properties of solids and a measure of stiffness. From Fig. 5, the additions of Sc, Ti, V, Cr, Mn, and Nb decreases the shear modulus and Young's modulus of Zr_5Sn_3. However, only the additions of Sc, Ga, and Ge decreases the bulk modulus. The Poisson's ratio (in Table 1) indicates the degree of directionality of the bonds atoms [36]. In general, the Poisson ratio is an important indicator to measure the degree of the covalent bonding and the value of ν is about 0.25 for ionic bonding, while as the small value of ν (0.1) implies covalent materials [37]. The calculated ν values of Zr_5Sn_3X are all larger than 0.19, which indicates that the bonding between atoms is mainly mixture of ionic type and metallic type. The Zr_5Sn_3Ga has the smallest Poisson's ratio and the strongest tendency of ionic and covalent bonding, and it has the largest Young's modulus among the 3rd long period elements, while Zr_5Sn_3Cr has the largest Poisson's ratio and the strongest metallic characteristics, then it has the lower Young's modulus. Among the considered elements, Zr_5Sn_3B has the largest Young's modulus and shear modulus.

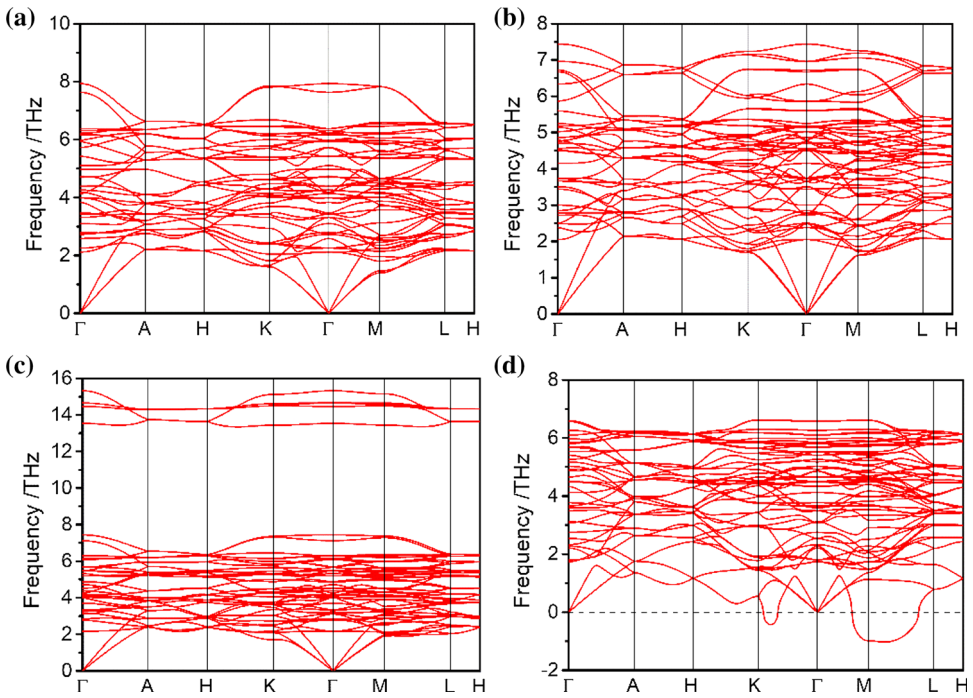

Figure 4 Phonon dispersion curves for **a** Zr_5Sn_3, **b** Zr_5Sn_4, **c** Zr_5Sn_3B and **d** Zr_5Sn_3Nb. The vibrational frequencies of Zr_5Sn_3, Zr_5Sn_4 and Zr_5Sn_3B are all positive and means the dynamical stability. However, the phonon dispersion curves of Zr_5Sn_3Nb include imagine frequencies along the high symmetric directions Γ–K, Γ–M, and L–M. This indicates that Zr_5Sn_3Nb is the dynamically unstable.

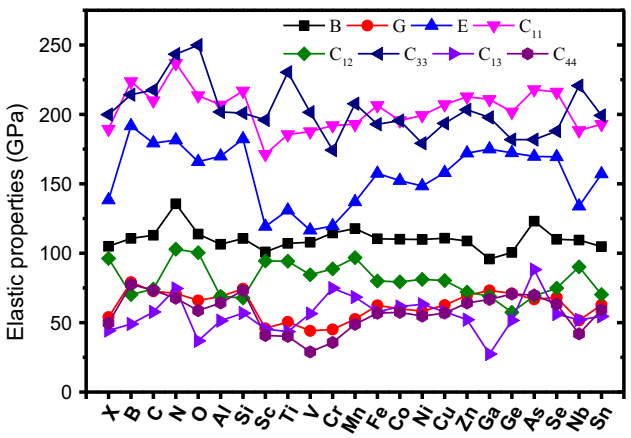

Figure 5 Elastic constants and elastic moduli of Zr_5Sn_3X.

Hardness

The Vickers hardness (H_v) has also been estimated with a theoretical model [38]: $H_v = 2(k^2G)^{0.585} - 3$, where k is the ratio of shear modulus and bulk modulus (G/B) and given in Table 1. The calculated H_v shows that the Zr_5Sn_3B has the largest hardness, while Zr_5Sn_3Cr has the lowest. The microscopic hardness correlates with the strength of chemical bond between atoms based on atomistic viewpoint. Some microscopic hardness models for materials of covalent bonding, ionic bonding and the mixture of them have been proposed, e.g., bond resistance, bond strength and electronegativity models [39]. As for intermetallic compound, it is hard to evaluate due to the delocation of interatomic interactions, and then the empirical model based elastic properties of alloy was used to predict the hardness. As mentioned above, the interatomic interactions between atoms for Zr_5Sn_3X are combination of ionicity (partially covalency) and metallicity. The bond strength of *s–p–d* hybridized chemical bond is greater than that of an *s-p* hybridized chemical bond [40]. The hybridization B-*p* with Zr2-*d* on the site is strongest, while that of Cr-*p*, Cr-*d* and Zr2-*d* is weakest in the Zr_5Sn_3X (see the discussion in electronic section). So Zr_5Sn_3B has the largest hardness, but Zr_5Sn_3Cr has the lowest hardness. The hardness is also correlated with the formation enthalpies of Zr_5Sn_3X. The more the negative formation enthalpy is, the largest the hardness is. From the calculated excess Gibbs formation free energy, Zr_5Sn_3Cr has the largest positive value indicating the lowest hardness. As for the excess Gibbs formation free energy of Zr_5Sn_3B is not the lowest compared with Zr_5Sn_3C, Zr_5Sn_3N, and Zr_5Sn_3O, but its Poisson's ratio is the largest among them, that means the covalent character is more important than the interatomic interaction.

Ductility

The ductility of a crystalline could be predicted via the Pugh ratio [41], the ratio between the bulk and the shear modulus, B/G. Pugh ratio is used empirically to predict brittle or ductile behavior of materials. In general, the ductility is positively correlated with the B/G value. If $B/G > 1.75$, the material behaves in a more ductile manner. On the contrary, the material behaves in a brittle manner if $B/G < 1.75$. From Table 1, it is notable that Zr_5Sn_3X (X = B, C, O, Al, Si, Zn, Ga, Ge, Se, Sn) characterize brittleness.

Anisotropy of elasticity

Mechanical anisotropies such as universal anisotropies A_U and anisotropies A_G and A_B [42] for Zr_5Sn_3X have been calculated as summarized in Table 1.

$$A_U = \frac{5G_V}{G_R} + \frac{B_V}{B_R} - 6; \quad A_G = \frac{G_V - G_R}{G_V + G_R} \times 100; \quad A_B = \frac{B_V - B_R}{B_V + B_R} \times 100 \tag{3}$$

It is found that the calculated A_G is less than A_B for Zr_5Sn_3X (X = B, Si, Co, Ni, Ge and Se), which suggests that the bulk modulus has a more directional dependence. From the calculated values of A_G and A_U, it is evident that Zr_5Sn_3 and Zr_5Sn_4 have directional dependence of shear modulus. The addition of other alloying element distinctly decreases the shear anisotropy except the elements O, Sc, Ti, V and Nb. The three-dimensional surfaces of mechanical moduli of Zr_5Sn_3 and Zr_5Sn_3X (X = B, Nb and Sn) are displayed in Fig. 6 and the rest (X = C, O, Al, Si, P, S, Cu, Zn, Ga, Ge, As, Fe, Co and Ni) are displayed in Figure S3 in Supplementary Information. The anisotropies of Zr_5Sn_3 and Zr_5Sn_3X (X = B, V, Ti, O, Cr and Nb) are strengthened. The surface contours of the Young's moduli for Zr_5Sn_3X are close to a sphere and their anisotropy of mechanical behavior is inconspicuous. This result agrees well with the aforementioned elastic constants.

Electronic density of states

The total density of states (TDOS) and partial density of states (PDOS) for some compounds (X = B, Nb and Sn) are shown in Fig. 6, and the rest (X = C, O, Al, Si, P, S, Cu, Zn, Ga, Ge, As, Fe, Co and Ni) are displayed in Figure S4 in Supplementary Information. In Fig. 6e, the states, which are approximately located between − 9.5 and − 6.5 eV below the Fermi level, originate from the bonding of Sn-*s* electrons, and the states located between − 4.5 and − 0.5 eV below the Fermi level originated from the bonding of Sn-*p* and Zr-*d*. The Fermi level lies in the pseudogap minimum, i.e., the bonding states are completely occupied. The bonding states are dominated by Sn-*s*, Sn-*p*, and Zr-*d*, while the antibonding states are dominated by Zr-*d* states. Below the Fermi level, Sn-*p* and Zr-*d* peaks show evidence for strong hybridization, while the other contributions are small.

For the Zr_5Sn_4 phase (Fig. 6f), it is found that the main bonding peaks between − 10 and − 6 eV are predominantly derived from Sn-*s* states, and the main bonding peaks between − 4.5 and 0 eV are dominated by Sn-*p* and Zr-*d* states, while the main antibonding peaks from 0 to 2.5 eV originate mainly from Zr-*d* states. Sn-*p* and Zr-*d* states show evidence for hybridization below the Fermi level. As for Zr_5Sn_3B (Fig. 6g), it is notable that the Fermi level locates at the local minimum of TDOS. That means the density of state at Fermi level is the lowest and it is the most stable. The other phases have PDOS similar to the ones of the Zr_5Sn_4 phase except that of Zr_5Sn_3Nb (see Fig. 6h). From Fig. 6h, one can see that there is peak positioned at 0.35 eV above Fermi level, which is similar as that of Zr_5Sn_3. This antibonding peak results in the instability of Zr_5Sn_3Nb relative Zr_5Sn_3.

Electronic bonding

The bonding properties provide insights into the alloying element effect. The bonding charge density plot is an important approach to visualize the nature of the bonds in addition to depict the charge transfer and the bonding properties. The bonding charge density is the difference between the self-consistent charge density and a reference charge density. This reference is a non-self-consistent charge density, which is computed from the super-position of the non-interacting atomic charge density when the atom positions are kept the same. The bonding charge densities of the considered phases have been calculated to insight the alloying mechanism and are depicted in Fig. 6i–l for Zr_5Sn_3, Zr_5Sn_3B, Zr_5Sn_3Nb, Zr_5Sn_3Sn, respectively, and the rest (X = C, O, Al, Si, P, S, Cu, Zn, Ga, Ge, As, Sc, Ti, V, Cr, Mn, Fe, Co and Ni) are displayed in Figure S5 in Supplementary

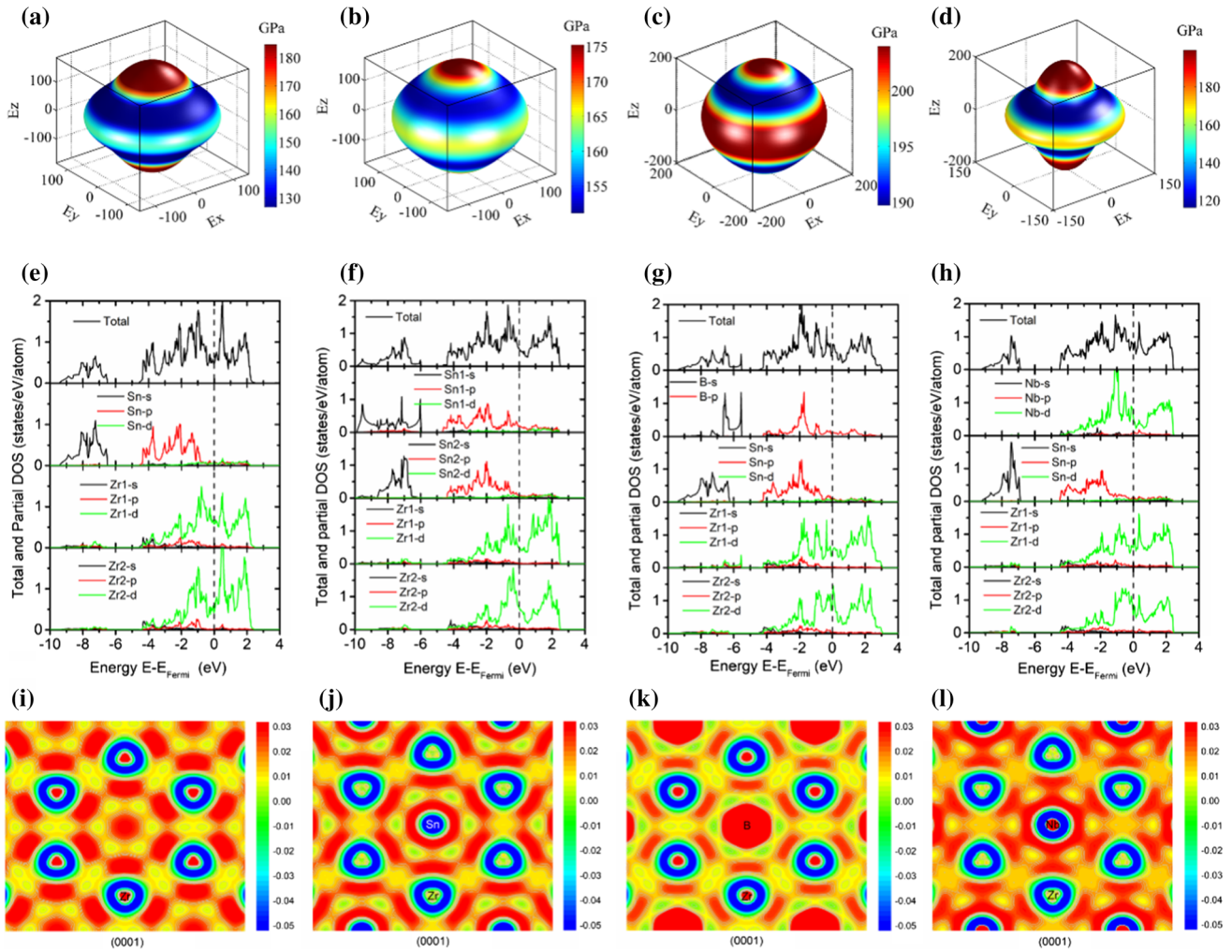

Figure 6 Directional dependence of Young's modulus for **a** Zr_5Sn_3, **b** Zr_5Sn_4, **c** Zr_5Sn_3B, **d** Zr_5Sn_3Nb. The anisotropy of Young's moduli for Zr_5Sn_4 and Zr_5Sn_3B is inconspicuous. The Young's modulus of Zr_5Sn_3Nb is dependent of direction. Total and partial density of states for the **e** Zr_5Sn_3, **f** Zr_5Sn_4, **g** Zr_5Sn_3B, **h** Zr_5Sn_3Nb. The addition of alloy element results in redistribution of Zr-*d* electrons. The addition of Sn or B increases the density of bonding state and reduces the density of antibonding state of Zr-*d* electrons, however, the addition of Nb does not change the distribution of Zr-*d* electrons near to Fermi level. Electronic density difference of the (i) Zr_5Sn_3, (j) Zr_5Sn_4, (k) Zr_5Sn_3B, (l) Zr_5Sn_3Nb. The accumulation of electron in the octahedral site in the Zr_5Sn_3. The effect of added B on the electronic density difference is negligible. But the addition of Sn excludes the electrons from the octahedral site. However, the addition of Nb results in the redistribution of electrons between Nb and Zr.

Information. The charge density changes with the addition of alloying elements, which results in the variation of electronic properties and mechanical behavior. It is clear that the charge accumulation among the Zr, Sn, and X (except X = Sc and Ti) atoms, which is an important reason for the higher elastic modulus compared with unalloyed Zr_5Sn_3. The addition of Sc, Ti, V, Cr, Mn, and Nb has a small effect on increasing the charge accumulation. The results indicate that the systems of Zr_5Sn_3X (X = Sc, Ti, V, Cr, Mn, and Nb) have lower elastic moduli compared with other alloys.

Debye temperature

The Debye temperature is an important quantity for the evaluation of thermodynamic properties of alloys. The calculated Debye temperatures of the Zr_5Sn_3X phases are summarized in Table 1. It is clear that Zr_5Sn_3B has the largest Debye temperature of 393.6 K, which means the Zr_5Sn_3B has a highest melting point among the considered compounds. The addition of alloying elements increases the Debye temperature except Sc, Ti, V, Cr, and Nb, for which the Debye temperature is lower than that of Zr_5Sn_3.

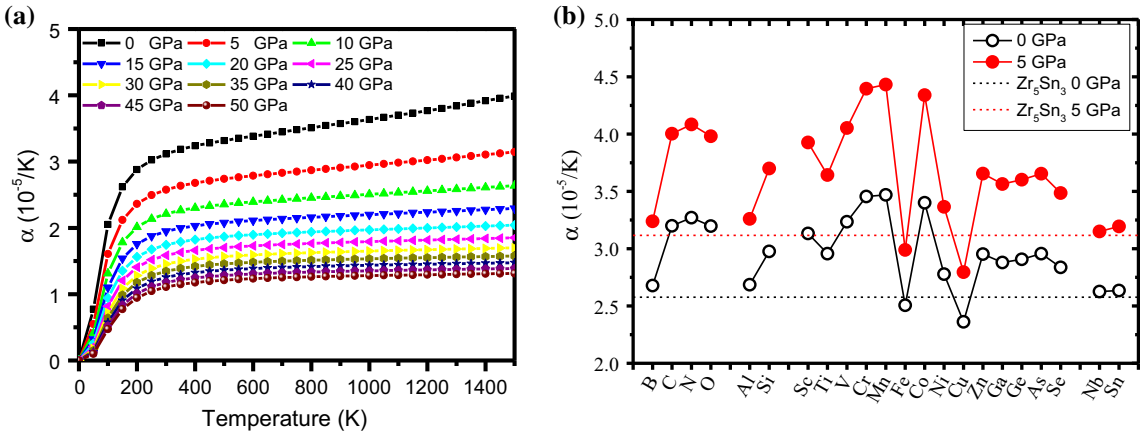

Figure 7 Bulk thermal expansion coefficient for **a** Zr_5Sn_3, **b** Zr_5Sn_3X at 300 K 0 GPa and 300 K 5 GPa. The thermal expansion increases with temperature and decreases with pressure. The addition of Fe or Cu reduces the thermal expansion of Zr_5Sn_3. The addition Cr, Mn, and Co increases remarkably the thermal expansion. However, the effect of Nb on the thermal expansion of Zr_5Sn_3 is negligible.

Thermodynamic properties

We have evaluated the thermodynamic properties in the temperature range of 0–1500 K and pressure from 0 to 50 GPa. The effect of temperature and pressure on the bulk thermal expansion coefficients of Zr_5Sn_3 are illustrated in Fig. 7a, and the rest (X = C, O, Al, Si, P, S, Cu, Zn, Ga, Ge, As, Sc, Ti, V, Cr, Mn, Fe, Co and Ni) are displayed in Figure S6 in Supplementary Information. The dependence of bulk thermal expansion coefficients of Zr_5Sn_3X on temperature and pressure are similar as that of Zr_5Sn_3. Figure 7b presents the bulk expansion coefficients of Zr_5Sn_3X (T = 300 K, P = 0, 5 GPa). It is clear that the bulk expansion coefficients of Zr_5Sn_3X (except X = Fe and Cu) are larger than that of Zr_5Sn_3. However, the bulk expansion coefficients of Zr_5Sn_3Cu and Zr_5Sn_3Fe are smaller than that of Zr_5Sn_3, which is due to their anisotropical change with addition alloying elements.

Bulk modulus at finite temperature and pressure

Figure 8a shows the dependence of bulk modulus of Zr_5Sn_3 on the temperature and pressure and those of Zr_5Sn_3X are given in Figure S7 in Supplementary Information. The bulk moduli of Zr_5Sn_3X at T = 300 K, and P = 0 and 5 GPa are presented in Fig. 8b. The figure shows that alloying elements (X = B, O, Al, Fe, Ni, Cu, Sn and Nb) increase the bulk modulus of Zr_5Sn_3. The other alloying elements decrease the value of the bulk modulus after alloying of Zr_5Sn_3.

Heat capacity on temperature and pressure

Figure 9a presents the specific heat capacity C_p versus temperature and pressure for Zr_5Sn_3, and those of Zr_5Sn_3X are given in Figure S8 in Supplementary Information. The specific heat capacity of Zr_5Sn_3 follows a general trend that it increases with temperature and decreases with pressure. The addition of alloying elements increases the heat capacity significantly (Fig. 9b), compared with the corresponding values of pristine Zr_5Sn_3.

Discussions

Zr_5Sn_3X, which is known as one of Nowotny phases with hexagonal structure, is one derivative of Mn_5Si_3 structure and is more stable than Zr_5Sn_3 except X = Sc, Ti, V, Cr, Mn, and Nb. The cell volume change of Zr_5Sn_3X relative to Zr_5Sn_3 is shown in Fig. 10a. The volume of added atom [43] was also included for comparison. The volume difference affected by adding the element is consistent with the volume of added atom except N and O, for which the volume of Zr_5Sn_3X attracted after addition. As for element Si, the volume of Zr_5Sn_3X is less than the total volume of Zr_5Sn_3 and X. The decrease in volume means that the more transfer of charge between the added atom and the matrix. Zr_5Sn_3O has the smallest

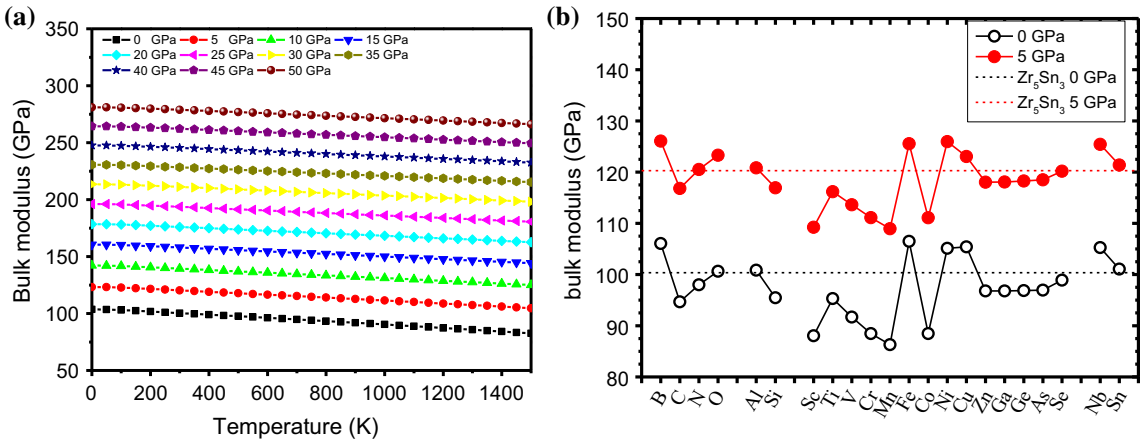

Figure 8 Bulk modulus for **a** Zr_5Sn_3, **b** Zr_5Sn_3X at T = 300 K and P = 0 and 5 GPa. The bulk modulus of Zr_5Sn_3 decreases with temperature and increases with pressure. The alloy elements B, Fe, Ni, Cu, and Nb result in increment of bulk modulus of Zr_5Sn_3. The addition O, Al and Sn do not change the bulk modulus. However, the other alloy elements considered decrease the bulk modulus, especially for Sc, Mn and Co.

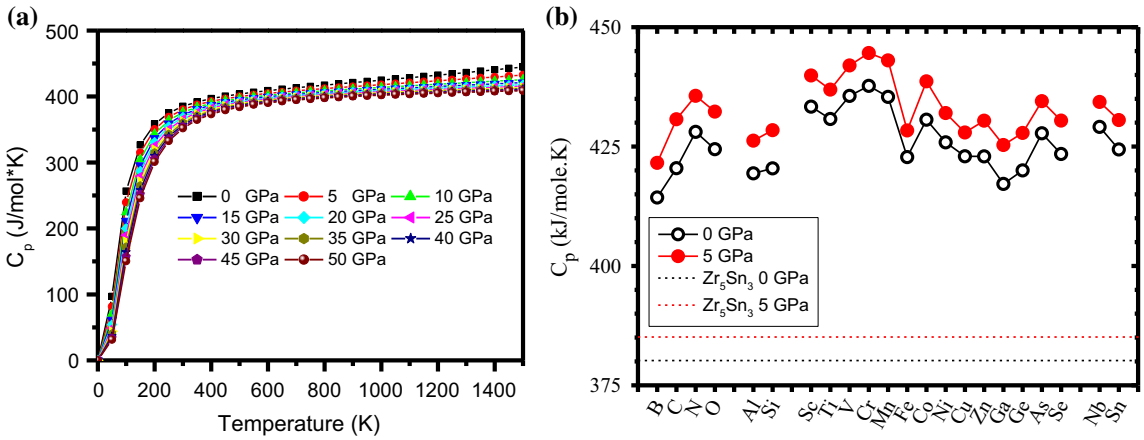

Figure 9 Specific heat capacity Cp for **a** Zr_5Sn_3, **b** Zr_5Sn_3X at T = 300 K and P = 0 and 5 GPa. The heat capacity of Zr_5Sn_3 increases as temperature increases but decreases with pressure. The alloying results in the apparent increment of heat capacity of Zr_5Sn_3.

volume and is the most stable from the point view of energetics. However, the Zr_5Sn_3Nb does not have the largest volume, but its excess formation enthalpy is positive, which means the stability of Zr_5Sn_3X is controlled not only the size factor but also the electronic factor. Namely, the alloying of Zr_5Sn_3 with element X increases the bonding and stability. For Zr_5Sn_3X systems, addition of X results charge transfer taking place from Zr to X (except X = Sc and Ti) (as shown in Fig. 2). One also can see that the Bader charge transferring from X is less than 0.5 and then the system has low stability, except complicated magnetic elements Cr and Mn. The analysis of the change in Bader charge indicates that the accommodation of Nb in Zr_5Sn_3Nb is the smallest due to the similar properties of Zr and Nb, and it has the lower stability. Compared with other alloying elements, with the addition of Nb, less charge transfers from Zr-2 to Nb, which corresponds the relatively weaker interaction between the Nb atoms and Zr-2 atoms. On the other hand, the elastic interaction is attributed the mismatch between the solute atom and the interstitial site of Zr_5Sn_3 when the solute atom embedding into the matrix and can be described using Eshelby formula [44]. Figure 10b demonstrates that the mapping counter of forming ability for Zr_5Sn_3X according to the elastic strain energy and Bader electron. One can see that the two parts was definitely segregated by a line. The system locating in the upper-left zone has positive excess formation enthalpy and this means

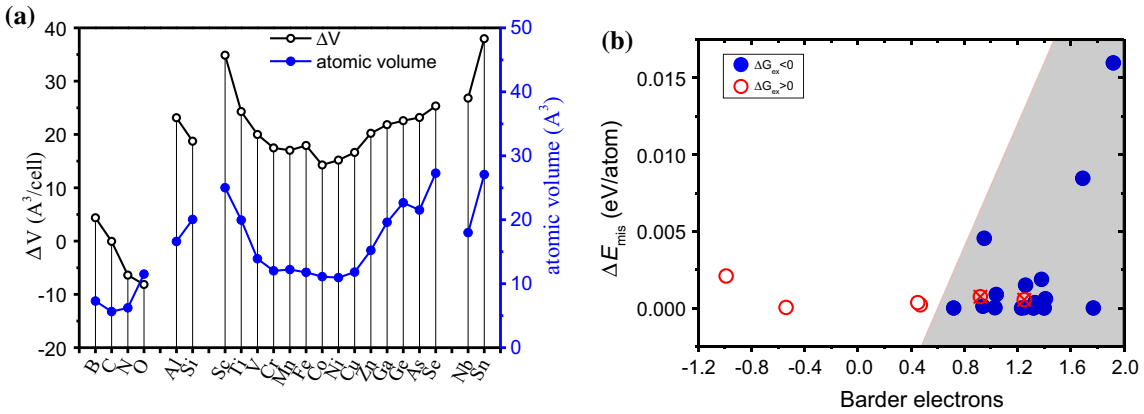

Figure 10 **a** Unit cell volumes difference (Å^3) between Zr_5Sn_3X and Zr_5Sn_3 as function of element. The atomic volume of element was also included. **b** The counter map of Zr_5Sn_3X forming ability. Two factors are included. One is the total transfer of electrons based on the analysis of Barder electron. The other is the elastic distortion energy due to lattice mismatch between the atomic radius of alloying element and the octahedral site. The red circle indicates the system Zr_5Sn_3X with negative excess Gibbs formation free energy and the blue filled circle represents system Zr_5Sn_3X the positive excess Gibbs formation free energy. The straight line was used to separate the two parts represent positive and negative excess Gibbs formation free energy. The regularity is good except two systems of Zr_5Sn_3Cr and Zr_5Sn_3Mn due to their magnetics.

that it does not form based on the point view of energetics. The right-down part is the forming zone of Zr_5Sn_3X. The elastic strain energy and Bader electron can be used to predict the forming ability of Zr_5Sn_3X. The two elements Cr and Mn do not satisfy the regularity (namely, the effects of factors on the forming tendency of Zr_5Sn_3X) due to their complex magnetic structure, although the calculated magnetic moment of Zr_5Sn_3X is small.

Conclusions

We investigate the interstitial chemistry engineering the properties of the Zr_5Sn_3 from first-principles. The effect of alloying element on the structural stability, elastic properties, and thermodynamic properties of Zr_5Sn_3 has been studied within the framework of density functional theory. The formation enthalpies of Zr_5Sn_3X are negative, which means that all are energetically stable relative to the correspondent pure constituents. The excess formation free energy between Zr_5Sn_3X and the mixture of Zr_5Sn_3 and alloying element X is also negative except X = Sc, Ti, V, Cr, Mn, and Nb, and this indicates that Zr_5Sn_3X is more stable than Zr_5Sn_3.

The elastic constants of Zr_5Sn_3X satisfy the mechanical stability criteria. The bulk moduli of Zr_5Sn_3X are larger than that of Zr_5Sn_3 except X = Sc, Ga, Ge and Sn. Zr_5Sn_3N has the highest bulk modulus. But Zr_5Sn_3B has the largest shear modulus, Young's modulus, Debye temperature, and microhardness. The addition of alloying element decreases the anisotropy except X = O, Sc, Ti, V, and Nb. The surface contours of the Young's moduli for Zr_5Sn_3X (except X = B, V, Ti, O, Cr, and Nb) are close to a sphere and their anisotropy of mechanical behavior is inconspicuous.

The specific heat capacity of Zr_5Sn_3X is larger than that of Zr_5Sn_3. The bulk expansion coefficients of Zr_5Sn_3Fe and Zr_5Sn_3Cu are lower than that of Zr_5Sn_3, while the others are larger. The elastic strain energy and Bader electron can be used to describe the forming ability of Zr_5Sn_3X. Our results could extend the knowledge of the tuning the structural, electronic, and mechanical properties of Zr_5Sn_3 with additive alloying elements, which could be helpful in designing and optimize the performance of Zr–Sn alloy under certain working conditions.

Acknowledgements

This work is financially supported by the National Natural Science Foundation of China (Grant Nos. 11464001, 51531009 and 51661003), the Guangxi Natural Science Foundation (2014GXNSFAA118308, 2016GXNSFBA380166).

Data availability

The datasets generated during and/or analyzed during the current study are available from the corresponding author on reasonable request.

Compliance with ethical standards

Conflict of interest There are no conflicts of interest to declare.

Electronic supplementary material: The online version of this article (https://doi.org/10.1007/s10853-019-03622-5) contains supplementary material, which is available to authorized users.

References

[1] Wei J, Frankel P, Polatidis E, Blat M, Ambard A, Comstock RJ, Hallstadius L, Hudson D, Smith GDW, Grovener CRM, Klaus M, Cottis RA, Lyon S, Preuss M (2013) The effect of Sn on autoclave corrosion performance and corrosion mechanisms in Zr–Sn–Nb alloys. Acta Mater 61:4200–4214

[2] Zhang R, Jiang B, Pang C, Dai X, Sun Y, Liao W, Wang Q, Dong C (2017) New low-Sn Zr cladding alloys with excellent autoclave corrosion resistance and high strength. Metals 7:144

[3] McPherson DJ, Hansen M (1953) The system zirconium–tin. Trans ASM 45:915–933

[4] Carpenter GJ, Ibrahim EF, Watters JF (1981) The aging response of zirconium–tin alloys. J Nucl Mater 102:280–291

[5] Arias D, Roberti L (1983) The solubility of tin in α and β zirconium below 1000 °C. J Nucl Mater 118:143–149

[6] Baykov VI, Perez RJ, Korzhavyi PA, Sundman B, Johansson B (2006) Structural stability of intermetallic phases in the Zr–Sn system. Scripta Mater 55(5):485–488

[7] Perez RJ, Toffolon-Masclet C, Joubert JM, Sundman B (2008) The Zr–Sn binary system: New experimental results and thermodynamic assessment. Calphad 32(3):593–601

[8] Krishna KM, Prakash DL, Timár G, Fitzner A, Srivastava D, Saibaba N, da Fonseca JQ, Dey GK, Preuss M (2016) The effect of loading direction and Sn alloying on the deformation modes of Zr: an in situ neutron diffraction study. Mater Sci Eng, A 650:497–509

[9] Liu S, Zhan Y, Wu J, Wei X (2015) Insight into structural, mechanical, electronic and thermodynamic properties of intermetallic phases in Zr–Sn system from first-principles calculations. J Phys Chem Solids 86:177–185

[10] Corbett JD, Garcia E, Guloy AM, Hurng WM, Kwon YU, Leon-Escamilla EA (1998) Widespread Interstitial Chemistry of Mn5Si3-Type and Related Phases: hidden Impurities and Opportunities. Chem Mater 10:2824–2836

[11] Garcia E, Corbett JD (1990) Chemistry in the polar intermetallic host zirconium antimonide, Zr5Sb3 Fifteen interstitial compounds. Inorg Chem 29:3274–3282

[12] Kwon YU, Corbett JD (1990) The zirconium–tin system, with particular attention to the Zr5Sn3-Zr5Sn4 region and Zr4Sn. Chem Mater 2:27–33

[13] Kwon YU, Corbett JD (1992) Influence of oxygen on the stability of zirconium–tin (Zr4Sn). Chem Mater 4:187–190

[14] Kwon YU, Corbett JD (1992) Chemistry in polar intermetallic compounds. The interstitial chemistry of zirconium–tin (Zr5Sn3). Chem Mater 4:1348–1355

[15] Balińska A, Kordan V, Misztal R, Pavlyuk V (2015) Electrochemical and thermal insertion of lithium and magnesium into Zr5Sn3. J Solid State Electrochem 19:2481–2490

[16] Blöchl PE (1994) Projector augmented-wave method. Phys Rev B 50:17953–17979

[17] Kresse G, Joubert D (1999) From ultrasoft pseudopotentials to the projector augmented-wave method. Phys Rev B 59:1758–1777

[18] Kresse G, Furthmüller J (1996) Efficient iterative schemes for ab initio total-energy calculations using a plane-wave basis set. Phys Rev B 54:11169–11186

[19] Kresse G, Furthmüller J (1996) Efficiency of ab initio total energy calculations for metals and semiconductors using a plane-wave basis set. Comput Mater Sci 6:15–50

[20] Perdew JP, Burke K, Ernzerhof M (1996) Generalized gradient approximation made simple. Phys Rev Lett 77:3865–3868

[21] Monkhorst HJ, Pack JD (1976) Special points for Brillouin-zone integrations. Phys Rev B 13:5188–5192

[22] Monkhorst HJ, Pack JD (1989) High-precision sampling for Brillouin-zone integration in metals. Phys Rev B 40:3616–3621

[23] Togo A. Phonopy. http://phonopy.sourceforge.net/

[24] Togo A, Oba F, Tanaka I (2008) First-principles calculations of the ferroelastic transition between rutile-type and $CaCl_2$-type SiO_2 at high pressures. Phys Rev B 78:134106

[25] Birch F (1947) Finite elastic strain of cubic crystals. Phys Rev B 71:809–824

[26] Blanco MA, Francisco E, Luana V (2004) GIBBS: isothermal-isobaric thermodynamics of solids from energy curves using a quasi-harmonic Debye model. Comput Phys Commun 158:57–72

[27] Wang SQ, Ye HQ (2003) Ab initio elastic constants for the lonsdaleite phases of C, Si and Ge. J Phys: Condens Matter 15:5307–5314

[28] Wu ZJ, Zhao EJ, Xiang HP, Hao XF, Liu XJ, Meng J (2007) Crystal structures and elastic properties of superhard IrN2

and IrN3 from first principles. Phys Rev B 76:054115-1–054115-15
[29] Voigt W (1928) Lehrbuch de Kristallphysik: Teubner-Leipzig. Macmillan, New York
[30] Reuss A (1929) Berechnug der Fließgrenze von Mischkristallen auf Grund der Plastizifäfsbedingung für Einkristalle. Angew Z Math Mech 9:49–58
[31] Hill R (1952) The elastic behaviour of a crystalline aggregate. Proc Phys Soc Lond. A 65:349–354
[32] Bader RFW (1990) Atoms in molecules: a quantum theory. Oxford University Press, Oxford
[33] Novotny H, Auer-Welsbach H, Bruss J, Kohl A (1959) Ein Beitrag zur M5Si3-Struktur (D88-Typ). Monatsh Chem 90:15–23
[34] Schubert K, Meissner HG, Raman A, Rossteutscher W (1964) Einige Strukturdaten metallischer Phasen. Naturewiss 51:287
[35] Meschel SV, Kleppa OJ (1998) Standard enthalpies of formation of some 3d, 4d and 5d transition-metal stannides by direct synthesis calorimetry. Thermochim Acta 314:205–212
[36] Yang J, Long J, Yang L, Li D (2013) First-principles investigations of the physical properties of binary uranium silicide alloys. J Nucl Mater 443:195–199
[37] Haines J, Leger JM, Bocquillon G (2001) Synthesis and design of superhard materials. Annu Rev Mater Res 31:1–23
[38] Chen XQ, Niu H, Li D, Li Y (2011) Modeling hardness of polycrystalline materials and bulk metallic glasses. Intermetallics 19:1275–1281
[39] Tian Y, Xu B, Zhao Z (2012) Microscopic theory of hardness and design of novel superhard crystals. Int J Refr Met Hard Mater 33:93–106
[40] Pauling L (1960) The nature of the chemical bond and the structure of molecules and crystals: an introduction to modern structural chemistry. Cornell University Press, New York
[41] Pugh SF (1954) Relations between the elastic moduli and the plastic properties of polycrystalline pure metals. Philos Mag 45:823–843
[42] Ravindran P, Fast L, Korzhavyi PA, Johansson B, Wills J, Eriksson O (1998) Density functional theory for calculation of elastic properties of orthorhombic crystals: application to TiSi2. J Appl Phys 84:4891–4904
[43] Compton WD, Gschneidner KA Jr, Hutchings MT, Rabin H, Tosi MP (1964) Physical properties and interrelationships of metallic and semimetallic elements. In: Seitz F, Turnbull D (eds) Solid state physics: advanced in research and applications, vol 16. Academic Press, New York, p 321
[44] Eshelby DJ (1954) Distortion of a crystal by point imperfections. J Appl Phys 25:255–261